10.2478/msr-2013-0038

MEASUREMENT SCIENCE REVIEW, Volume 13, No. 5, 2013

Design and Analysis of a Novel Six-Component F/T Sensor based on CPM for Passive Compliant Assembly

Qiaokang Liang[1], Dan Zhang[2], Yaonan Wang[1], Yunjian Ge[3]

[1]College of Electric and Information Technology, Hunan University, Changsha, Hunan 410082, China, qiaokang@mail.ustc.edu.cn

[2]Faculty of Engineering and Applied Science, University of Ontario Institute of Technology, Oshawa, Ontario, Canada L1H 7K4, dan.zhang@uoit.ca

[3]State Key Laboratories of Transducer Technology, Institute of Intelligent Machines, Chinese Academy of Science, Hefei, Anhui 230031, China, yjge@iim.ac.cn

This paper presents the design and analysis of a six-component Force/Torque (F/T) sensor whose design is based on the mechanism of the Compliant Parallel Mechanism (CPM). The force sensor is used to measure forces along the *x*-, *y*-, and *z*-axis (F_x, F_y and F_z) and moments about the *x*-, *y*-, and *z*-axis (M_x, M_y and M_z) simultaneously and to provide passive compliance during parts handling and assembly. Particularly, the structural design, the details of the measuring principle and the kinematics are presented. Afterwards, based on the Design of Experiments (DOE) approach provided by the software ANSYS®, a Finite Element Analysis (FEA) is performed. This analysis is performed with the objective of achieving both high sensitivity and isotropy of the sensor. The results of FEA show that the proposed sensor possesses high performance and robustness.

Keywords: Compliant Parallel Mechanism, Passive Compliant Assembly, Six-component F/T sensor.

1. INTRODUCTION

SINCE the Oak Ridge and Argonne National Laboratories applied force feedback on the load the slave manipulator encountered to their master-slave manipulator during the late 1940s, F/T sensing with appropriate control techniques has played an important role in the dexterous and reliable robotic manipulation. After F/T control has been recognized as a key scheme for using robots in advanced applications [1], various types of F/T sensors have been designed and developed [2-6]. Several six-axis force sensors are commercially available at present, such as force sensors of ATI [7] and JR3.

A major problem in developing force sensors is the design of the force-sensing element, which has been done heuristically, dependent on the experience of designers [1]. To detect three orthogonal forces and three orthogonal torques simultaneously, the force-sensing elements of multi-component force sensors are always featured by complicated geometrical structures, which make accurate calculation of strains and deflection difficult or even impossible with current techniques. Another critical drawback of the traditional multi-component F/T sensor is the existence of significant measurement couplings among components, especially between component M_x and component F_y, component M_y and component F_x. Additionally, as there are six components to be measured and processed simultaneously, approximately equal measurement sensitivity for each component is expected [8], [9]. Furthermore, the stiffness and the sensitivity of the F/T sensor is always a trade-off, which means users have to make a sacrifice of stiffness to get a high-sensitivity performance and vice versa.

Taking into account the above-mentioned drawbacks, researchers found that parallel mechanisms are preferred to be considered as a candidate for a force-sensing element of a multi-component F/T sensor due to their following advantages [6].

1. Relative maturity of the theory system: all the related theory, such as position analysis, statics, stiffness analysis, dynamics, have been investigated for a long time and gotten well known;
2. Possibility to provide decoupling F/T information: unlike traditional force-sensing elements that sense all F/T components with a single monolithic structure, force-sensing elements based on parallel mechanisms employ their limbs to sense the components and show a limited cross talk;
3. Isotropy: based on the statics analysis of parallel mechanisms, a global stiffness matrix denoting the relationship between the undergoing load and the infinitesimal movement of the mobile platform can be obtained, which could be used to pursue measurement isotropy among components;
4. High stiffness and high sensitivity: as the stiffness of the robotic manipulator depends on the component with minimum stiffness, which is always the F/T sensor, the stiffness of a F/T sensor is a critical performance factor. However, it is impossible for a traditional force-sensing element of high stiffness to detect F/T with high sensitivity. On the contrary, for the force-sensing element based on parallel mechanisms, the limb stiffness can be much lower compared to the overall required stiffness of the F/T sensor due to their parallel arrangement. Therefore, the trade-off between stiffness and sensitivity can be solved.

Recently, some researchers developed force/torque sensors based on parallel mechanisms to meet the requirement and escape the mentioned shortcoming [6]. Gailet and Reboulet developed a force sensor of SP (Stewart Platform) based on octahedral structure [10]. Dwarakanath and Bhaumick designed and implemented a force/torque sensor based on the SP structure in 1999, and the analysis deals with kinematic design, leg design and optimization of the form of the leg and the aspects of integration were presented [11].

Table 1. Comparisons on the multi-dimensional F/T sensor.

Year & developer	Fabrication technology	Size (mm) & No. of axes	Sensitivity & Measurement range	Sensing principle
1998 & Jin and Mote	Bulk silicon micro-machining and wafer-bonding technologies	4.5 × 4.5 × 1.2 & 6	1 mN and 2 mN mm for force and moment components (resolutions) & n.a.	Piezo-resistive
1999 & Mei et al.	CMOS process, silicon bulk micro-machining	4×4×2 & 3	13mV/N in the Z-axis and about 2.3mv/N in X- and Z-axis & 0—50 N in Z-axis, ±10N in X- and Y-axis	Piezo-resistive
2012 & Brookhuis, Lammerink	Bulk silicon Micro-machining and silicon fusion bonding	9×9×1 (PCB chip) & 3	16 PF/N in Fz and 2.7PF/N mm in Mx and My & 50N in Fz, ±25 N mm in Mx and My	Capaci-tive
2009 & Takenawa, S.	Four chip inductors, silicone gel, and a neodymium magnet	3.2× 2.5 × 2.2 & 3	0.06 N (resolution) & -40 N to 40 N	Inducti-ve
2011 & M. Gobbi et al.	Three spoke structure, standard mechanical machining	40.25× 16 × 16 & 6	95% (uncertainty) & 10 kN (Fz), 5 kN (Fx, Fy) and 0.5 kNm (M)	Strain gauge
2004 & Liu, Inoue et al.	Parallel support mechanism & machining	170×10 5×26.5 & 6	Fx=Fy=20kgf, Fz=l00kgf, and Mx=My=Mz=l0 0 Nm	Strain gage
1990 & Hirose and Yoneda	Three elastomers in a flexed spoke shape & milling and electric discharge machining	Φ76×4 0 & 6	0.3% & 100 kgf and 300kgfcm for parallel and rotating directions, respectively	Optical
2010 & Jia, Lin, and Liu	Stewart platform & standard mechanical machining	small than Φ160 × 210	linear error and the repeatability error of 1%, interference error of 4.5% & 40kN and 5kNm for force and moment components	Piezo-electric

Ranganath, Mruthyunjaya and Ghosal analyzed and designed a SP-based force/torque sensor in a near-singular configuration with high sensitivity [12]. Nguyen, Antrazi and Zhou presented the kinematic analysis of a 6 DOF force/torque sensor based on the mechanism of the Stewart Platform and composed of two platforms coupled together by 6 spring-loaded pistons [13]. Dasgupta, Reddy and Mruthyunjaya presented a design methodology for the Stewart Platform sensor structure based on the optimal conditioning of the force transformation matrix [14]. Hou, Zeng, Yao et al. presented a six-component F/T sensor based on a hyperstatic Stewart Platform. Parameter optimization of the sensor structure was performed with genetic algorithms, and the sensor shows good isotropy and sensitivity performances [15]. Recently, Jia, Lin, and Liu introduced another type of Stewart Platform dedicated to heavy six-axis load sharing measurement [16], [17]. With single-component force piezoelectric sensor fixed in each limb, the sensor could measure six-component F/T with linear and repeatability error of 1%. The comparisons of main features and characterization methods using a selection of multi-dimensional F/T sensors up to the date of the publication are shown in Table 1.

Unfortunately, in force-sensing applications, the presence of clearance, friction and backlash at the rigid mechanical joints of parallel mechanisms will modify the axial forces that the limbs are subjected to, therefore, disturb the performance of the sensor in unpredictable ways. To avoid these problems, force-sensing candidate based on parallel mechanism is preferred to be designed with flexural joints, which eliminate the friction, backlash and wear and possess sub-micron accuracy with high resolution, continuous and smooth displacement.

In this paper, modeling and performance evaluation of a novel six-component force/torque sensor based on compliant parallel mechanism is presented, which consists of three identical sensing limbs of type SPS (Spherical-Prismatic-Spherical) and one central leg with three degrees of freedom. The compliant joints of the four limbs are employed as active force-sensing portions. By the electric measurement technique of strain gauge, the developed sensor can provide high-performance force/torque information, and the calibration experiment shows that the presented sensor possesses positive characteristics such as high stiffness and sensitivity, weak couplings, and good isotropy.

2. ARCHITECTURE DESCRIPTION OF THE SENSOR

The proposed force-sensing element is based on spatial parallel compliant mechanism with three identical sensing limbs of type SPS and one central limb with three DOFs connecting the mobile platform and the base. Each sensing limb consists of two three-axis flexural joints as spherical joints at its both ends and a one-axis flexural joint as a prismatic joint in the middle. After neglecting the redundant degrees of freedom about the lines passing through the two spherical joints, the total degree of freedom of each limb is equal to six. Therefore, these limbs impose no constraint on the moving platform. The central limb consists of a large-displacement compliant universal joint and a large-displacement compliant revolute joint, and it has connectivity of three and imposes three constraints on the moving platform. Fig.1. shows a 3D model of the proposed sensor.

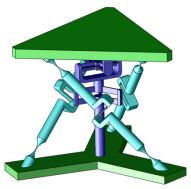

Fig.1. Six-component force/torque sensor based on compliant parallel mechanism.

Fig.2. shows the link-pair relationship diagram for the 3-DOF mechanism. The blue boxes represent passive joints while the red boxes represent sensing joints, which are used as the elastic element of the sensor. The number of degrees of freedom, F_d, is given by the Chebyshev-Grubler-Kutzbach criterion:

$$F_d = \lambda(n-j-1)+\sum_{i=1}^{j} f_i - f_r = 6\times(9-11-1)+24-3=3 \quad (1)$$

Where λ denotes the dimension of the space, n and j denote the number of links and the number of joints, respectively, f_i and f_r represent the degree of freedom associated with joint i and the number of redundant degrees of freedom in the mechanism.

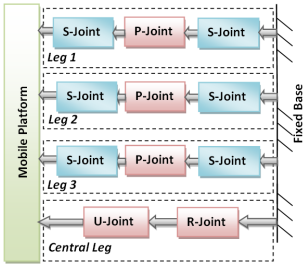

Fig.2. Schematic diagram of the compliant parallel mechanism.

The notch hinges and the leaf type flexure are probably the most popular element in applications of compliant mechanisms. All compliant joints used in this design are shown in Fig.3.

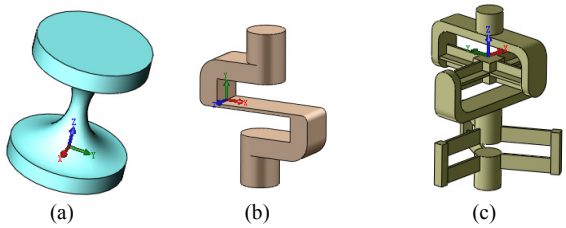

(a) (b) (c)

Fig.3. Compliant joints used in the design: (a) compliant spherical joint; (b) compliant prismatic joint; (c) compliant spherical joint for central limb.

Toroidal notch hinge, as shown in Fig.3(a)., is commonly utilized in spatial compliant mechanisms to provide 3-axis motions [25], [26]. The equation for the stiffness in the freedom axes can be approximated from [27], [28].

$$\frac{M_y}{\theta_y}=\frac{M_x}{\theta_x}\approx\frac{Et^{7/2}}{20R^{1/2}} \quad (2)$$

$$\frac{F_x}{\theta_y}=\frac{F_y}{\theta_x}\approx\frac{Et^{7/2}}{20R^{3/2}} \quad (3)$$

$$\frac{F_z}{\delta_z}\approx\frac{Et^{3/2}}{2R^{1/2}} \quad (4)$$

Where F_n and δ_n are the force and translation displacement in n-axis, respectively; t and R are the inter-hole space and common radius of notches, respectively; and M_n and θ_n are the moment and rotational displacement around n-axis, respectively; the E is modulus of longitudinal elasticity of the material.

The majority of the existing compliant translational joints are based on a parallel four-bar building block [29]. Though they can deliver a pure translational motion with acceptable off-axis stiffness, the range of motion is very limited and the construction is complicated. A novel compliant translational joint based on a simple cantilever is proposed and shown in Fig.3(b).

Due to its geometry character (as shown in Fig.4.), the applied force F_y is transmitted to the beam through a drive bar with an additional bending moment M_z. The bending equation for this particular leaf spring is given by

$$EI\frac{d^2\delta_y}{dx^2}=F_y\frac{L}{2}-F_y(L-x)=F_y(x-\frac{L}{2}) \quad (5)$$

Integrating twice with boundary conditions and assuming small displacements, then,

$$EI\theta=F_y(\frac{1}{2}x^2-\frac{L}{2}x) \quad (6)$$

$$EI\delta_y=F_y(\frac{1}{6}x^3-\frac{L}{4}x^2) \quad (7)$$

The slope and deflection at the free end of the beam can be obtained

$$\theta\big|_{x=L}=\frac{F_y}{EI}(\frac{1}{2}x^2-\frac{L}{2}x)=0 \quad (8)$$

$$\delta_y\big|_{x=L}=\frac{F_y}{EI}(\frac{1}{6}x^3-\frac{L}{4}x^2)=-F_y\frac{L^3}{12EI} \quad (9)$$

The compliant spherical joint for central limb used in this study, which was designed by Trease [25], [26], is shown in Fig.3(c).

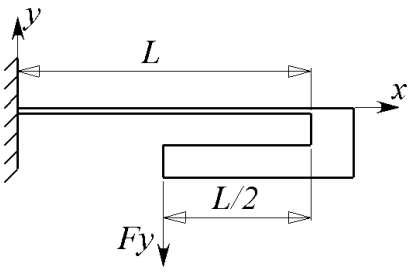

Fig.4. The configuration of the cantilever.

3. KINEMATICS

The pseudo-rigid-body model provides a simple method of analyzing compliant systems that undergo large, nonlinear deflections and is used to model the deflection of flexible members using rigid-body components that have equivalent force-deflection characteristics. Therefore, rigid-link mechanism theory may be used to analyze the compliant mechanism [31], [32].

A. Inverse and forward kinematics

Fig.5. shows a kinematically equivalent diagram of the proposed micro-manipulator, in which squares and cylinders represent prismatic and revolute joints, respectively. The lower ends of the actuated limbs, points A_1, A_2, A_3, are connected to fixed base through universal joints, and the upper end of the actuated limbs, points P_1, P_2, P_3, are connected to the mobile platform through spherical joints.

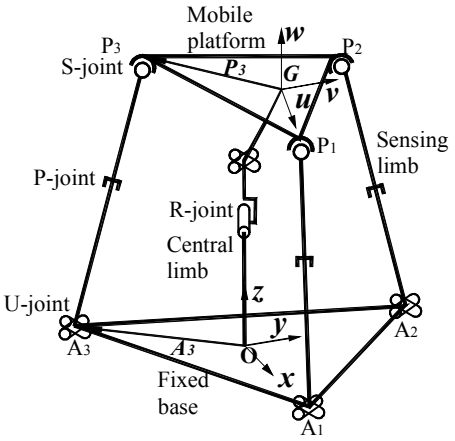

Fig.5. Kinematically equivalent diagram of the sensor.

As shown in Fig.6., the fixed base reference frame $O_{\{x, y, z\}}$ and the mobile coordinate frame $G_{\{u, v, w\}}$ are attached to the fixed base and the mobile platform, respectively. The original of the $O_{\{x, y, z\}}$ is located at the centroid O of the triangle $A_1A_2A_3$, which is the original placement without displacement, and the x- and y-axis lying on the triangle plane with y-axis parallel to A_3A_2 and x-axis pointing to A_1. The original of the $G_{\{u, v, w\}}$ is located at the centroid G of the triangle $P_1P_2P_3$ with the u and v-axis lying on the triangle plane and u-axis pointing to P_1 and v-axis parallel to P_3P_2. Triangles $P_1P_2P_3$ and $A_1A_2A_3$ are set equilateral with the lengths q and e, respectively.

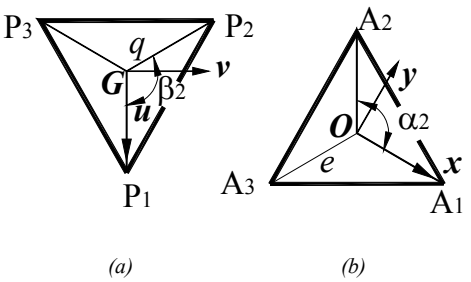

Fig.6. Top views of the mobile platform (a) and the base (b).

The angle α_i, β_i represent the angle between x-axis and the line OA_i and the angle between u-axis and the line PP_i, respectively. So, the position vector A_i with respect to frame O and P_i with respect to frame G can be written as

$$A_i = [e \cdot c\alpha_i \quad e \cdot s\alpha_i \quad 0]^T, \text{ for } i=1, 2, 3 \tag{10}$$

$$P_i = [q \cdot c\beta_i \quad q \cdot s\beta_i \quad 0]^T, \text{ for } i=1, 2, 3 \tag{11}$$

As the platform of the mechanism has three degrees of freedom, only three of the six Cartesian coordinates of the platform are independent, which have been chosen for convenience as (ψ, θ, Φ).

The position of the moving platform is defined by the vector, $\boldsymbol{G}$,

$$\boldsymbol{G} = \overline{OG} = \begin{bmatrix} G_x & G_y & G_z \end{bmatrix}^T \tag{12}$$

And the orientation of the moving platform is defined by the rotation matrix,

$${}^{O}R_P = R_z(\phi)R_y(\theta)R_x(\psi) \tag{13}$$

Where ψ, θ, Φ (roll, pitch and yaw angles) represent three successive rotations of the moving frame about the fixed x, y and z-axis [33]. As the passive limb is a 3-DOF serial chain, its posture can be described by the three joint variables, θ_1, θ_2, θ_3. Referring to Fig.7., the coordinate frames are established and the corresponding Denavit-Hartenberg parameters are given in Table 2.

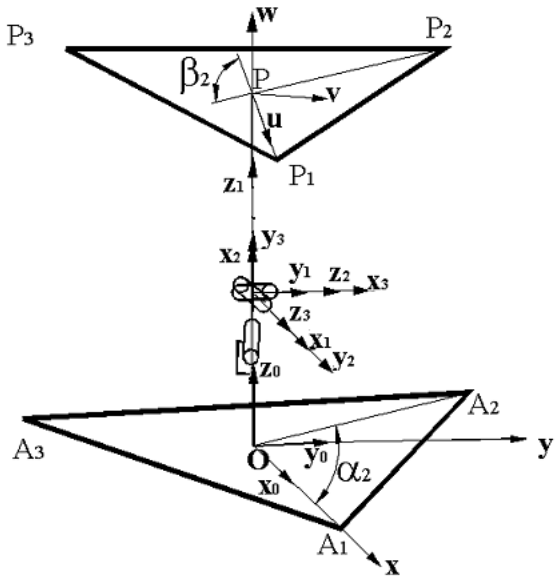

Fig.7. Coordinate frames of the central limb.

Hence, the D-H transformation matrices from the moving platform to the fixed base can be obtained [33].

Table 2. The D-H parameters of the passive constraining limb.

i	a_i	d_i	α_i	θ_i
1	0	l_1	0	θ_1
2	0	0	-π/2	θ_2
3	0	0	-π/2	θ_3
G	0	l_4	0	0

$$
{}^{O}T_P = T_1T_2T_3T_P = \begin{bmatrix} {}^{O}R_P & {}^{O}G \\ 0 & 1 \end{bmatrix}
$$
$$
= \begin{bmatrix} c\theta_1c\theta_2c\theta_3 \\ +s\theta_1s\theta_3 & c\theta_1s\theta_2 & c\theta_1c\theta_2s\theta_3 \\ -s\theta_1c\theta_3 & l_4(-c\theta_3s\theta_1 \\ +c\theta_1c\theta_2s\theta_3) \\ s\theta_1c\theta_2c\theta_3 \\ -c\theta_1s\theta_3 & s\theta_1s\theta_2 & s\theta_1c\theta_2s\theta_3 \\ -s\theta_1c\theta_3 & l_4(c\theta_1c\theta_3 \\ +c\theta_2s\theta_1s\theta_3) \\ s\theta_2c\theta_3 & -c\theta_2 & s\theta_2s\theta_3 & l_1+l_4s\theta_2s\theta_3 \\ 0 & 0 & 0 & 1 \end{bmatrix} \quad (14)
$$

Comparing (13) to (14), one can yield

$$
\theta_2 = cos^{-1}(c\theta s\psi) \quad (15)
$$

$$
\theta_3 = Atan2(\frac{s\theta c\psi}{s\theta_2}, \frac{-s\theta}{c\theta_2}) \quad (16)
$$

$$
\theta_1 = Atan2(\frac{s\phi s\theta s\psi + c\phi c\psi}{s\theta_2}, \frac{s\phi c\theta}{s\theta_2}) \quad (17)
$$

The inverse kinematics problem can be simply stated as: given the independent parameters, ψ, θ, Φ, to find the corresponding lengths of the actuated limbs:

$$
d_i = \sqrt{[G - A_i + {}^{O}R_P\,{}^{P}P_i]^T[G - A_i + {}^{O}R_P\,{}^{P}P_i]} \quad (18)
$$

For the forward kinematics, the limb lengths l_1, l_2, and l_3 are given and the problem is to find the orientation of the mobile platform. (18) is written in the following form [33]:

$$
\begin{aligned} &\mu_{i1}c\theta_1c\theta_2c\theta_3 + \mu_{i2}s\theta_1c\theta_2c\theta_3 + \mu_{i3}s\theta_1s\theta_3 \\ &+ \mu_{i4}c\theta_1s\theta_3 + \mu_{i5}s\theta_1s\theta_2 + \mu_{i6}c\theta_1s\theta_2 \text{ for } i=1, 2, 3 \\ &+ \mu_{i7}c\theta_3s\theta_3 + \mu_{i8}c\theta_2 + \mu_{i9} = 0 \end{aligned} \quad (19)
$$

Where μ_{ij} are constant coefficients that are determined by the manipulator geometry and input leg lengths [33].

B. Jacobian matrix

Since the mechanism possesses only three rotational degrees of freedom, the input vector can be written as the extension rate of the sensing limbs $\dot{\mathbf{d}} = \left[\dot{d}_1, \dot{d}_2, \dot{d}_3\right]^T$, and the output vector can be presented as the angular velocity of the moving platform, $\dot{\mathbf{X}} = \left[\omega_x, \omega_y, \omega_z\right]^T$ By using the velocity vector-loop method, we can obtain the Jacobian matrix of the mechanism A without the passive leg,

$$
A\dot{\mathbf{X}} = \dot{\mathbf{d}} \quad (20)
$$

Where

$$
A = \begin{bmatrix} \mathbf{s}_1^T & \left(\mathbf{P}_1 \times \mathbf{s}_1\right)^T \\ \mathbf{s}_2^T & \left(\mathbf{P}_2 \times \mathbf{s}_2\right)^T \\ \mathbf{s}_3^T & \left(\mathbf{P}_3 \times \mathbf{s}_3\right)^T \end{bmatrix} \quad (21)
$$

And $\boldsymbol{s}_i$ is the unit vector pointing along the ith limb.

The Jacobian matrix of the passive constraining leg of the mechanism $\boldsymbol{B}$ can be expressed as

$$
B = \begin{bmatrix} e_1 & e_2 & e_3 \\ e_1 \times r_1 & e_2 \times r_2 & e_3 \times r_3 \end{bmatrix}
$$
$$
= \begin{bmatrix} l_4(-c\theta_1c\theta_3 \\ -c\theta_2s\theta_1s\theta_3) & l_4c\theta_1s\theta_2s\theta_3 & l_4(c\theta_1c\theta_2c\theta_3 \\ +s\theta_1s\theta_3) \\ l_4(-s\theta_1c\theta_3 \\ -c\theta_1c\theta_2s\theta_3) & -l_4s\theta_2s\theta_1s\theta_3 & l_4(c\theta_2c\theta_3s\theta_1 \\ -c\theta_1s\theta_3) \\ 0 & l_4c\theta_2s\theta_3 & l_4c\theta_3s\theta_2 \\ 0 & s\theta_1 & c\theta_1s\theta_2 \\ 0 & -c\theta_1 & c\theta_1s\theta_2 \\ 1 & 0 & -c\theta_2 \end{bmatrix} \quad (22)
$$

Hence,

$$
\dot{\theta}_1 = c\theta_1\frac{c\theta_2}{s\theta_2}\omega_1 + s\theta_1\frac{c\theta_2}{s\theta_2}\omega_2 + \omega_3 \quad (23)
$$

$$
\dot{\theta}_2 = s\theta_1\omega_1 - c\theta_1\omega_2 \quad (24)
$$

$$
\dot{\theta}_3 = \frac{c\theta_1}{s\theta_2}\omega_1 + \frac{s\theta_1}{s\theta_2}\omega_2 \quad (25)
$$

J, a 3x3 Jacobian matrix, relating the independent velocity variables of mobile platform, $\dot{\mathbf{X}}$, to the vector of sensing limb rates, $\dot{\mathbf{d}}$.

$$
\dot{\mathbf{d}} = A\begin{bmatrix} J_s \\ I_{3\times3} \end{bmatrix}\dot{\mathbf{X}} = AJ_t\dot{\mathbf{X}} = J\dot{\mathbf{X}} \quad (26)
$$

Where, J_t, a 6×3 Jacobian matrix, relating the velocity state of the moving platform, $\mathbf{v}_G = \begin{bmatrix} \dot{G}_x & \dot{G}_y & \dot{G}_z \end{bmatrix}^T$, to the vector of sensing limb extension rates. And J_s, a 3×3 Jacobian matrix, relating the three independent velocities $\dot{\mathbf{X}}$ to the three dependent velocities $\mathbf{v}_G$, which could be obtained through (22) to (25).

4. MEASURING PRINCIPLE

Several measurement techniques have been used to transduce the interaction between a contacting load and a F/T sensor into multi-dimensional force and torque. The transduction method which has received most attention in F/T sensor design is concerned with the conductive and resistive approach. Strain gauges commonly act as sensing elements on devices for measuring force in conductive and resistive approach. The measurement chain consists of several elements from true load to measured F/T, as shown in Fig.8. The succession of conversions for a single strain gauge is the following.

1) Load to elastic strain: mechanical stress occurs when load F acts on the elastic element of the sensor, and specific deformation and elastic strain will occur accordingly, following the Hook's law of elasticity. The quality of the occurred stain ε only relates to the applied force/torque F after the dimensions of the force-sensing element are decided.

$$\varepsilon = \chi(F) \tag{27}$$

2) Elastic strain to variation of resistance: occurred strain will result in variation of relative resistance of strain gauges bonded on the force-sensing element. The gauge factor, denoted by G_f, is defined mathematically as follows [34].

$$G_f = \frac{\Delta R/R}{\varepsilon} \tag{28}$$

where R is the original resistance of the strain gauge. Therefore, the resistance change ΔR of the resistance of the strain gauge is:

$$\Delta R = G_f \cdot R \cdot \chi(F) \tag{29}$$

3) Resistance change to output voltage variation: Full-bridge circuits, as a ratiometric device, increase further the sensitivity of the circuit. And its measurement sensitivity is:

$$\frac{\Delta U}{U} = -G_f \cdot \varepsilon = -G_f \cdot \chi(F) \tag{30}$$

Where ΔU and U are output of the circuit and voltage excitation source, respectively.

4) Voltage output to F/T output: besides common signal conditioning and signal processing, nonlinear decoupling and calibration are necessary due to the nonlinear coupling error, which seriously decreases the sensor measurement precision..

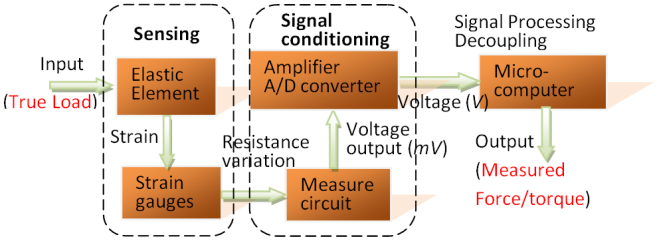

Fig.8. Structure of measurement chain.

When resistive moments are exerted on the mobile platform, the compliant prismatic joints in each sensing limb are compressed or extended. Therefore, the moving platform possesses three degrees of freedom in micro-scale spherical motion. Hence the force sensor can provide passive compliance to the mobile platform during parts assembly. By the virtual work principle, we can obtain

$$\boldsymbol{w}^T \Delta X = \boldsymbol{f}^T \Delta d \tag{31}$$

where $\boldsymbol{w}=[M_x, M_y, M_z]^T$ is the vector of the moment applied to the platform, and $\boldsymbol{f}=[f_1,f_2,f_3]^T$ represents the force that the sensing limb is subjected to. Where $\Delta X, \Delta d$ represent the vector of virtual displacements associated with the mobile platform and sensing limbs, respectively. (31) can be rewritten as

$$\boldsymbol{w}^T \dot{\boldsymbol{X}} = \boldsymbol{f}^T \dot{\boldsymbol{d}} \tag{32}$$

Substituting (26) into (32) yields

$$\boldsymbol{w} = J^T \boldsymbol{f} \tag{33}$$

Hence the moments applied on the moving platform can be calculated from the actuated limb forces, and vice versa.

A. Attachment of position of stain gauges

The central limb restricts the sensor's freedom of displacements along *x*-, *y*-, and *z*-axis. Therefore, the force F_x, F_y, and F_z applied on the mobile platform will be transmitted through the central limb. Finite Element Analysis (FEA) via software ANSYS® was performed and the distributions of the normal elastic strains occurring on the CPM under sign-dimensional force/torque are shown in the Fig.9.

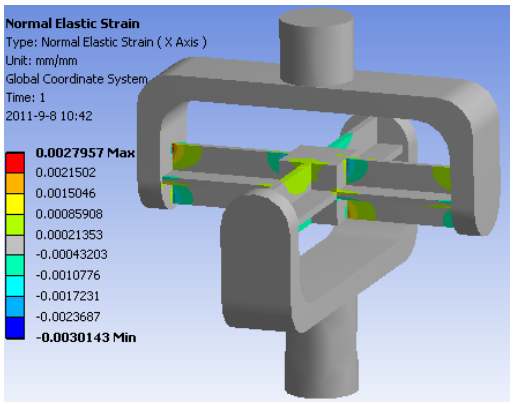

(a)

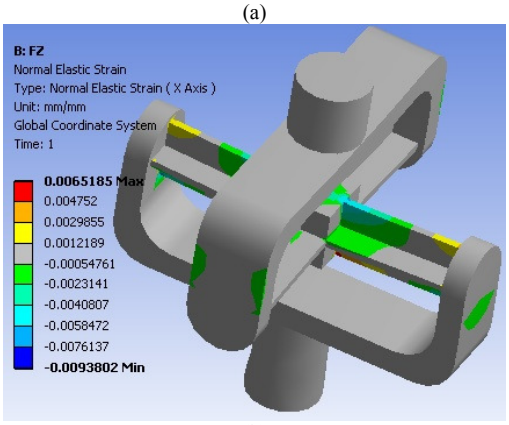

(b)

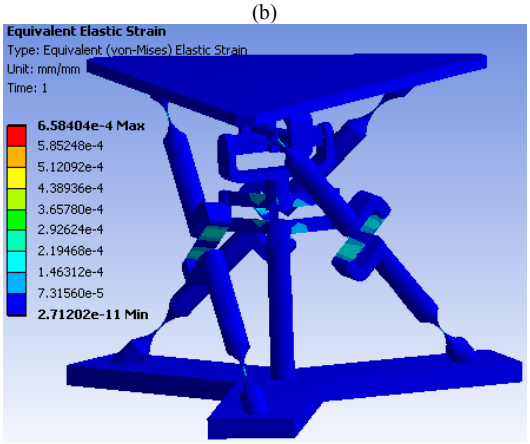

(c)

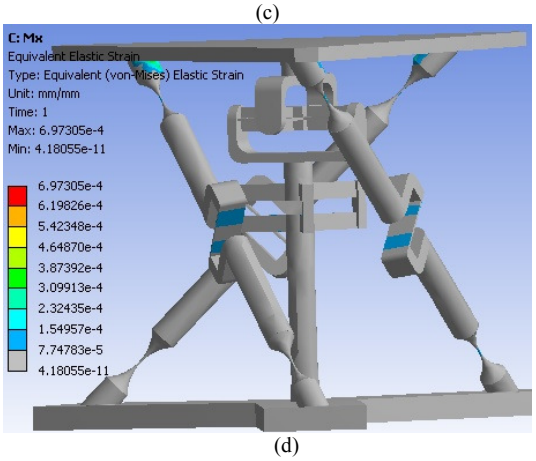

(d)

Fig.9. The strain produced in the CPM by the force F_x (a), the force F_z (b), the moment M_x (c) and M_z (d).

Spots that have the maximum strain are selected to bond strain gauges to detect the corresponding loads, as shown in Fig.10.

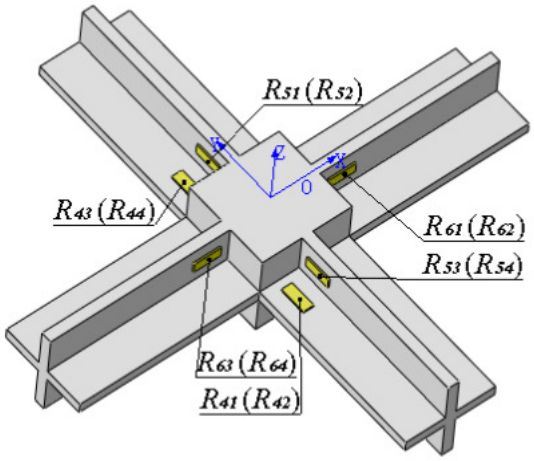

(a)

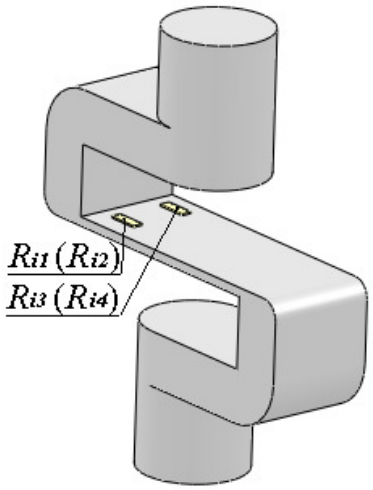

(b)

Fig.10. Strain gauges arrangement: (a) arrangement on the sensing limbs; (b) arrangement on the central limb.

B. Connection mode of strain gauges

According to the arrangement scheme of strain gauges, the Wheatstone bridges connection mode of the sensor is determined, as shown in Fig.11. All of the gauges used in the present study are Y series linear strain gauges (1-LY11-3/120) made by HBM Inc.

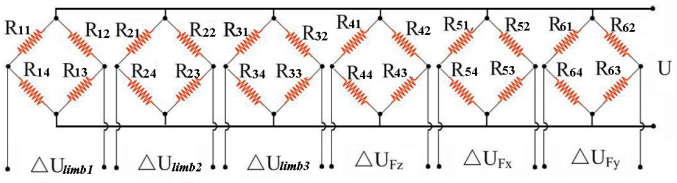

Fig.11. Wheatstone bridges connection mode.

When the sensor is applied to single force/torque F_x, F_y, F_z respectively, corresponding output of each bridge is:

$$\begin{aligned}\Delta U_{Fz} &= \frac{U}{4}\left(\frac{\Delta R_{41}}{R_{41}}-\frac{\Delta R_{42}}{R_{42}}+\frac{\Delta R_{43}}{R_{43}}-\frac{\Delta R_{44}}{R_{44}}\right)\\ &= \frac{U}{4}\left(2\left(\frac{\Delta R_{41}}{R_{41}}\right)_{\varepsilon}-2\left(\frac{\Delta R_{42}}{R_{42}}\right)_{\varepsilon}\right)\\ &= \frac{UK}{2}(\varepsilon_{41}+|\varepsilon_{42}|)\end{aligned} \tag{34}$$

$$\begin{aligned}\Delta U_{Fx} &= \frac{U}{4}\left(\frac{\Delta R_{51}}{R_{51}}-\frac{\Delta R_{52}}{R_{52}}+\frac{\Delta R_{53}}{R_{53}}-\frac{\Delta R_{54}}{R_{54}}\right)\\ &= \frac{U}{4}\left(2\left(\frac{\Delta R_{51}}{R_{51}}\right)_{\varepsilon}-2\left(\frac{\Delta R_{52}}{R_{52}}\right)_{\varepsilon}\right)\\ &= \frac{UK}{2}(\varepsilon_{51}+|\varepsilon_{52}|)\end{aligned} \tag{35}$$

$$\begin{aligned}\Delta U_{Fy} &= \frac{U}{4}\left(\frac{\Delta R_{61}}{R_{61}}-\frac{\Delta R_{62}}{R_{62}}+\frac{\Delta R_{63}}{R_{63}}-\frac{\Delta R_{64}}{R_{64}}\right)\\ &= \frac{U}{4}\left(2\left(\frac{\Delta R_{61}}{R_{61}}\right)_{\varepsilon}-2\left(\frac{\Delta R_{62}}{R_{62}}\right)_{\varepsilon}\right)\\ &= \frac{UK}{2}(\varepsilon_{61}+|\varepsilon_{62}|)\end{aligned} \tag{36}$$

Where K is the sensitivity coefficient of the strain gauges, ε_i is the elastic strain at the spot where the R_i is bonded on the diaphragms, U is the excitation voltage, and $\Delta R_i/R_i$ means change rate of the resistance of the strain gauge R_i due to strain variation.

The corresponding output of each sensing limb can be calculated as

$$\begin{aligned}\Delta U_{\text{limb1}} &= \frac{U}{4}\left(\frac{\Delta R_{11}}{R_{11}}-\frac{\Delta R_{12}}{R_{12}}+\frac{\Delta R_{13}}{R_{13}}-\frac{\Delta R_{14}}{R_{14}}\right)\\ &= \frac{U}{4}\left(2\left(\frac{\Delta R_{11}}{R_{11}}\right)_{\varepsilon}-2\left(\frac{\Delta R_{12}}{R_{12}}\right)_{\varepsilon}\right)\\ &= \frac{UK}{2}(\varepsilon_{11}+|\varepsilon_{12}|)\end{aligned} \tag{37}$$

$$\begin{aligned}\Delta U_{\text{limb2}} &= \frac{U}{4}\left(\frac{\Delta R_{21}}{R_{21}}-\frac{\Delta R_{22}}{R_{22}}+\frac{\Delta R_{23}}{R_{23}}-\frac{\Delta R_{24}}{R_{24}}\right)\\ &= \frac{U}{4}\left(2\left(\frac{\Delta R_{21}}{R_{21}}\right)_{\varepsilon}-2\left(\frac{\Delta R_{22}}{R_{22}}\right)_{\varepsilon}\right)\\ &= \frac{UK}{2}(\varepsilon_{21}+|\varepsilon_{22}|)\end{aligned} \tag{38}$$

$$\begin{aligned}\Delta U_{\text{limb3}} &= \frac{U}{4}\left(\frac{\Delta R_{31}}{R_{31}}-\frac{\Delta R_{32}}{R_{32}}+\frac{\Delta R_{33}}{R_{33}}-\frac{\Delta R_{34}}{R_{34}}\right)\\ &= \frac{U}{4}\left(2\left(\frac{\Delta R_{31}}{R_{31}}\right)_{\varepsilon}-2\left(\frac{\Delta R_{32}}{R_{32}}\right)_{\varepsilon}\right)\\ &= \frac{UK}{2}(\varepsilon_{31}+|\varepsilon_{32}|)\end{aligned} \tag{39}$$

5. COMPLIANCE/STIFFNESS ANALYSIS

The compliance of the CPM can be established via a proper investigation by taking into account the flexibilities of every compliant joint [27], [28], [29], [30]. In what follows, the compliance of the developed CPM based on the stiffness matrix method is presented.

With the definition of local z-axis in Fig.3., the infinitesimal translational and rotational displacements X of mobile platform are formulated when the load F is exerted on a certain point, given the linear relation between the applied load and deformation.

$$\begin{aligned}X &= [\delta x, \delta y, \delta z, \theta x, \theta y, \theta z]^T\\ &= CF = C[Fx, Fy, Fz, Mx, My, Mz]^T\end{aligned} \tag{40}$$

where $\boldsymbol{C}$ is the compliance matrix of the CPM.

Each limb of a parallel mechanism can be considered as a serial chain that comprises m joints, which are assumed to be flexure members with the local compliance matrix c_{ij} - established in the local frame. Given the deformations only relate to the compliant joints, we can obtain the lumped deformation at the tip of the ith limb

$$X_i = \sum_{j=1}^{m} x_{ijR} = \sum_{i=1}^{m} J_{ij} x_{ij} \tag{41}$$

where x_j and x_{jR} are the elastic deformations of the flexure member of the chain with respect to the local and the reference frame, respectively. And J_{ij} can be derived as follows:

$$J_{ij} = \begin{bmatrix} R_{ij} & -R_{ij}S(\mathbf{r}_{ij}) \\ 0 & R_{ij} \end{bmatrix} \tag{42}$$

which requires knowledge of the position $\boldsymbol{r_{ij}}$ of the origin of reference frame with respect to local frame as well as the orientation R_{ij} of reference frame with respect to local frame. And $S(*)$ is the skew-symmetric operator.

Similarly, the wrench F_i applied on the tip of the ith limb described in the reference frame can be distributed to wrenches f_{ij} on the jth flexure member of the ith limb:

$$f_{ij} = J_{Fij} F_i \tag{43}$$

Where $J_{Fij} = J_{ij}^{T}$. From (26) and (29)

$$X_i = C_i F_i = \sum_{j=1}^{m} J_{ij} x_{ij} = \sum_{j=1}^{m} J_{ij} c_{ij} f_{ij} = \sum_{j=1}^{m} J_{ij} c_{ij} J_{ij}^{T} F_i \tag{44}$$

Therefore, the compliance of the ith limb is given by

$$C_i = \sum_{j=1}^{m} J_{ij} c_{ij} J_{ij}^{T} \tag{45}$$

From the kinematic analysis, the mobile platform and tips of limbs have the same angular displacements but different linear displacements. Particularly, the displacement vector of the CPM in X and the displacement vector of the tip of the ith limb X_i can be transformed reciprocally,

$$X = J_i X_i \tag{46}$$

where J_i is the transformation matrix from the reference of ith limb, whose reference point is set at the tips of limbs, to the reference of the CPM. Similarly, the wrench F applied on the platform described in the reference frame of CPM can be obtained via distributed wrench F_i described in the reference frame of the limbs

$$F = KX = \sum_{i=1}^{n} J_{Fi} F_i \tag{47}$$

where J_{Fi} is the transformation matrix of the applied wrench from the local frame to the reference frame:

$$J_{Fi} = J_i^T = \begin{bmatrix} R_i & 0 \\ S(\mathbf{r}_i)R & R_i \end{bmatrix} \tag{48}$$

Let K and k_i be the stiffness matrix of the CPM and the stiffness of the ith limb, respectively. Form (42) and (43), one can obtain

$$F = KX = \sum_{i=1}^{n} J_{Fi} F_i = \sum_{i=1}^{n} J_{Fi} K_i X_i = \sum_{i=1}^{n} J_i^T K_i J_i^{-1} X \tag{49}$$

Then, the stiffness of the CPM becomes

$$K = \sum_{i=1}^{n} J_i^T K_i J_i^{-1} \tag{50}$$

6. FINITE ELEMENT ANALYSIS

Finite Element Analysis (FEA) via software ANSYS® was performed to certify that the sensor possesses appropriate sensitivity and compliance. The normal strains in the locations of strain gauges are listed in Table 3. when the sensor undergoes single component load.

The measurement sensitivity defined as the ratios of the output voltages to the input voltages can be obtained by using the strain results listed in Table 3. [4]. Sufficient measuring isotropy among components ensures that the electrical circuit of a multi-component sensor possesses amplification symmetry, high degree of integration and simple decoupling methods. The Anisotropy index of the sensor is calculated by using the obtained measurement sensitivities. These are listed in Table 4.

When resistive or gravitational forces/torques are exerted on the mobile platform, the compliant spherical joint in the central leg and the compliant prismatic joints in each sensing limb are compressed or extended. As a consequence, the CPM is also able to provide passive compliance to the mobile platform during parts handling and assembly. The displacements of the sensor are indicated in Fig.12. when it is subjected to the single rated component force/torque. By calculating, the maximum displacements/rotations it can provide are 0.071 mm along x-axis, 0.008 mm along z-axis, and 0.085° about x-axis, and 0.018° about z-axis.

Table 3. Normal strains in the locations of strain gauges.

	F_x=1N	F_y=1N	F_z=1N	M_x=10N·mm	M_y=10N·mm	M_z=10 N·mm
ε_{11}	-2.57 e-5	2.259 e-5	-4.80 e-5	2.856 e-4	-2.821 e-4	-1.967 e-4
ε_{12}	2.497 e-5	-2.22 e-5	4.801 e-5	-2. 781 e-4	2.827 e-4	1.9736 e-4
ε_{13}	-2.61 e-5	2.301 e-5	-4.80 e-5	2.861 e-4	-2.812 e-4	-2.105 e-4
ε_{14}	2.526 e-5	-2.29 e-5	4.798 e-5	-2.859 e-4	2.819 e-4	2.0982 e-4
ε_{21}	-1.09 e-5	-1.10 e-5	-4.80 e-5	-2.732 e-4	2.601 e-7	-2.132 e-4
ε_{22}	1.102 e-5	1.101 e-5	4.879 e-5	2.728 e-4	-2.594 e-7	1.9861 e-4
ε_{23}	-1.12 e-5	-1.11 e-5	-4.80 e-5	-2.709 e-4	2.610 e-7	-2.110 e-4
ε_{24}	1.241 e-5	1.239 e-5	4.799 e-5	2.173 e-4	-2.598 e-7	2.1092 e-4
ε_{31}	2.261 e-5	-2.56 e-5	-4.80 e-5	2.571 e-7	2.863 e-4	-1.985 e-4
ε_{32}	-2.21 e-5	2.486 e-5	4.802 e-5	-2.497 e-7	-2. 871 e-4	1.9842 e-4
ε_{33}	2.312 e-5	-2.61 e-5	-4.80 e-5	2.586 e-7	2.874 e-4	-2.098 e-4
ε_{34}	-2.29 e-5	2.524 e-5	4.797 e-5	-2.579 e-7	-2.869 e-4	2.1025 e-4
ε_{41}	-5.43 e-5	4.481 e-5	3.157 e-4	-5.892 e-8	2.502 e-7	3.586 e-6
ε_{42}	-4.74 e-5	4.931 e-5	-2.95 e-4	5.886 e-8	-2.509 e-7	-3.58 e-6
ε_{43}	-5.63 e-5	4.627 e-5	3.207 e-4	7.028 e-8	-2.839 e-7	-3.22 e-6
ε_{44}	-5.70 e-5	4.692 e-5	-3.14 e-4	-7.019 e-8	2.849 e-7	3.211 e-6
ε_{51}	-3.25 e-4	1.590 e-5	1.134 e-4	2.497 e-7	1.598 e-6	-1.56 e-5
ε_{52}	2.999 e-4	1.621 e-5	1.136 e-4	-2.499 e-7	-1.611 e-6	1.556 e-5
ε_{53}	-2.97 e-4	-2.19 e-5	1.141 e-4	-2.847 e-7	1.798 e-6	-1.07 e-5
ε_{54}	2.982 e-4	-2.70 e-5	1.142 e-4	2.851 e-7	-1.792 e-6	1.110 e-5
ε_{61}	1.611 e-5	-3.23 e-4	1.129 e-4	1.644 e-6	-5.901 e-8	-1.07 e-5
ε_{62}	1.601 e-5	3.109 e-4	1.139 e-4	-1.651 e-6	5.890 e-8	1.112 e-5
ε_{63}	-2.17 e-5	-3.09 e-4	1.140 e-4	1.838 e-6	7.031 e-8	-1.57 e-5
ε_{64}	-2.06 e-5	3.072 e-4	1.139 e-4	-1.829 e-6	-7.021 e-8	1.561 e-5

Table 4. Measurement sensitivity and anisotropy index of the sensor (Gauge Factor K=2.1).

Measurement sensitivities (S_i)	F_x	F_y	F_z	f_1	f_2	f_3
ΔU/U (mV/V)	1.281	1.318	1.267	1.192	1.184	1.207
Isotropy index $\frac{Max\{S_i\} - Min\{S_i\}}{\sqrt{\sum_6 S_i^2 / 6}}$	0.107846					

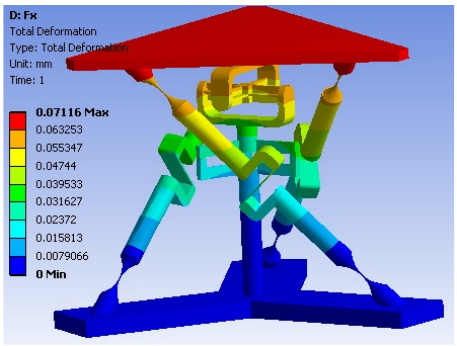

(a)

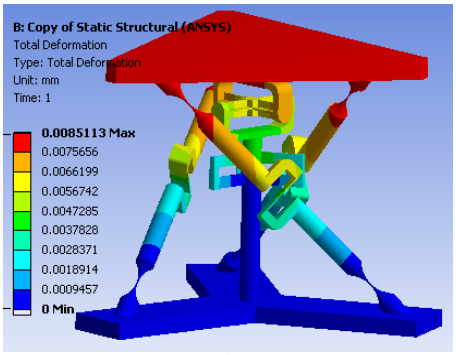

(b)

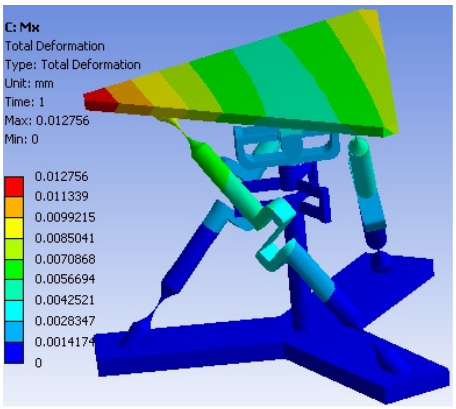

(c)

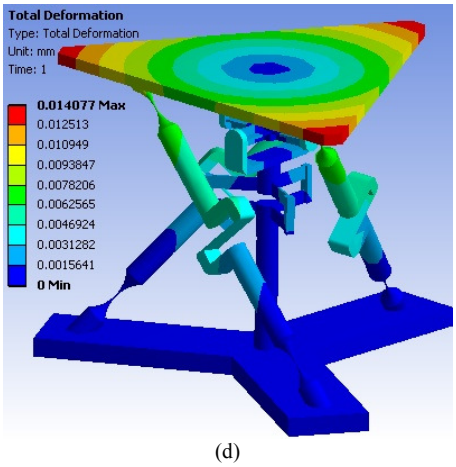

(d)

Fig.12. The flexible deformation of the CPM under applied force F_x=1N (a), the force F_z=1N (b), the moment M_x =0.05N·m(c) and M_z =0.05 N·m (d).

7. CALIBRATION METHOD AND DECOUPLING MATRIX

Calibration is used to adjust the output voltages of the electrical circuit to agree with the value of the applied standard within a specified accuracy [35]. Besides, the majority of the existing multi-component force/torque sensors are confronted by high coupled interference errors among their six components, especially between component F_x and component M_y, component F_y and component M_x respectively, which need a complicated calibration and decoupling test to get the decoupling matrix. With the analysis mentioned in Section 4 and the method proposed in [35], [36], [37], the decoupling matrix C of the proposed sensor can be obtained.

$$F = CS = \begin{bmatrix} \lambda I_{3\times3} & C_1 \\ C_2 & \lambda J \end{bmatrix} S \tag{51}$$

Where the S is the output of the bridge circuits, λ is the linear coefficient between output of the bridge circuits to standard load, and C_1 and C_2 represent the influence between the three moment components and the three force components.

8. CONCLUSIONS AND FUTURE WORK

This study has endeavored to design and analyze a novel six-component force/torque sensor based on the mechanism of CPM. The sensor is used to measure six-component force/torque simultaneously and to provide passive compliance during in parts handling and assembly. The sensing element of the sensor is newly modeled using a monolithic CPM. The kinematic transformations for the force sensor, the measuring principle and compliance analysis are introduced. The FEA is performed and its results show that the proposed sensor possesses high sensitivity, good isotropy, simple decoupling method and moderate compliance.

Further activities will be devoted to the dynamic analysis and automatic manipulation based on real-time computation of forces and torques. Moreover, fabrication and extensive experimentation of the six-component F/T sensor based on the proposed CPM is planned. Finally, an experimental platform integrated with driver, the developed sensor, and control algorithm will be developed.

ACKNOWLEDGMENT

This work was supported in part by the National Nature Science Foundation of China (NSFC 61203207), specialized Research Fund for the Doctoral Program of Higher Education (No. 20120161120015), Hunan province Science and Technology Planning Project of China (2012RS4046) and China Postdoctoral Science Foundation (2012M510189, 2013T60768). The second author appreciates the financial support from Natural Sciences and Engineering Research Council of Canada (NSERC).

REFERENCES

[1] Nakamura, Y., Yoshikawa, T., Futamata, I. (1998). Design and signal processing of six-axis force sensors. In *Robotics Research : The Fourth International Symposium.* MIT Press, 75-81.

[2] Kim, J.H., Kang, D.I., Shin, H.H., Park, Y.K. (2003). Design and analysis of a column type multi-component force/moment sensor. *Measurement*, 33, 213-219.

[3] Kim, G.S. (2001). The design of a six-component force/moment sensor and evaluation of its uncertainty. *Measurement Science and Technology*, 12 (9), 1445-1455.

[4] Hashimoto, K. et al. (2013). Overload protection mechanism for 6-axis force/torque sensor. In *Romansy 19 – Robot Design, Dynamics and Control*. Springer, Vol. 544, 383-390.

[5] Liu, S.A., Tzo, H.L. (2002). A novel six-component force sensor of good measurement isotropy and sensitivities. *Sensors and Actuators A: Physical*, 100 (2-3), 223-230.

[6] Liang, Q., Zhang, D., Wang, Y., Coppola, G., Ge, Y. (2013). PM based multi-component F/T sensors—state of the art and trends. *Robotics and Computer-Integrated Manufacturing*, 29 (4), 1-7.

[7] ATI Industrial Automation. *Multi-axis force / torque sensors*. http://www.ati-ia.com/products/ft/sensors.aspx.

[8] Baki, P., Szekely, G., Kosa, G. (2012). Miniature tri-axial force sensor for feedback in minimally invasive surgery. In *Biomedical Robotics and Biomechatronics (BioRob) : 4th IEEE RAS & EMBS International Conference*, 24-27 June 2012. IEEE, 805-810.

[9] Mastinu, G., Gobbi, M., Previati, G. (2011). A new six-axis load cell. Part I: Design. *Experimental Mechanics*, 51 (3), 373-388.

[10] Gailler, A., Reboulet, C. (1983). An isostatic six component force and torque sensor. In *13th International Symposium on Industrial Robots and Robots 7*, 17-21 April 1983. Robotics International of SME.

[11] Dwarakanath, T.A., Bhaumick, T.K., Venkatesh, D. (1999). Implementation of Stewart platform based force-torque sensor. In *Multisensor Fusion and Integration for Intelligent Systems (MFI '99) : IEEE/SICE/RSJ International Conference,* 15-18 August, 1999, 32-37.

[12] Ranganath, R., Nair, P.S., Mruthyunjaya, T.S., Ghosal, A. (2004). A force-torque sensor based on a Stewart platform in a near-singular configuration. *Mechanism and Machine Theory*, 39 (9), 971-998.

[13] Nguyen, C., Antrazi, S., Zhou, Z. (1991). Analysis and implementation of a 6 DOF Stewart platform-based force sensor for passive compliant robotic assembly. In *IEEE Proceedings of Southeastcon '91*, 7-10 April 1991. IEEE, 880-884.

[14] Dasgupta, B., Reddy, S., Mruthyunjaya, T.S. (1994). Synthesis of a force–torque sensor based on the Stewart platform mechanism. In *Proceedings of the National Convention of Industrial Problems in Machines and Mechanisms*, Bangalore, India, 14-23.

[15] Hou, Y., Zeng, D., Yao, J., Kang, K., Lu, L., Zhao, Y. (2009). Optimal design of a hyperstatic Stewart platform-based force/torque sensor with genetic algorithms. *Mechatronics*, 19 (2), 199-204.

[16] Jia, Z.Y., Lin, S., Liu, W. (2010). Measurement method of six-axis load sharing based on the Stewart platform. *Measurement*, 43 (3), 329-335.

[17] Liu, W., Li, Y.J., Jia, Z.Y., Zhang, J., Qian, M. (2011). Research on parallel load sharing principle of piezoelectric six-dimensional heavy force/torque sensor. *Mechanical Systems and Signal Processing*, 25 (1), 331-343.

[18] Jin, W.L., Mote, C.D., Jr. (1998). A six-component silicon micro force sensor. *Sensors and Actuators A: Physical*, 65 (2-3), 109-115.

[19] Mei, T., Ge, Y., Chen, Y., Ni, L., Liao, W.H., Xu, Y., Li, W.J. (1999). Design and fabrication of an integrated three-dimensional tactile sensor for space robotic applications. In *Micro Electro Mechanical Systems (MEMS '99) : 12th IEEE International Conference*, 17-21 January 1999. IEEE, 112-117.

[20] Brookhuis, R.A., Lammerink, T.S.J., Wiegerink, R.J., de Boer, M.J., Elwenspoek, M.C. (2012). 3D force sensor for biomechanical applications. *Sensors and Actuators A: Physical*, 182, 28-33.

[21] Takenawa, S. (2009). A soft three-axis tactile sensor based on electromagnetic induction. In *Mechatronics 2009. ICM 2009 : IEEE International Conference*, 14-17 April 2009. IEEE, 1-6.

[22] Liu, T., Inoue, Y., Shibata, K., Yamasaki, Y., Nakahama, M. (2004). A six-dimension parallel force sensor for human dynamics analysis. In *Robotics, Automation and Mechatronics*, 1-3 December 2004. IEEE, 208-212.

[23] Hirose, S., Yoneda, K. (1990). Development of optical six-axial force sensor and its signal calibration considering nonlinear interference. In *Robotics and Automation*, 13-18 May 1990. IEEE, 46-53.

[24] Gobbi, M., Previati, G., Guarneri, P., Mastinu, G. (2011). A new six-axis load cell. Part II: Error analysis, construction and experimental assessment of performances. *Experimental Mechanics*, 51 (3), 389-399.

[25] Trease, B.P., Moon, Y.M., Kota, S. (2005). Design of large-displacement compliant joints. *ASME Journal of Mechanical Design*, 127, 788-798.

[26] Zhu, Z.H., Meguid, S.A. (2008). Vibration analysis of a new curved beam element. *Journal of Sound and Vibration*, 309 (1), 86-95.

[27] Wu, T., Chen, J., Chang, S. (2008) A six-DOF prismatic-spherical-spherical parallel compliant nanopositioner. *IEEE Transactions on Ultrasonics Ferroelectrics and Frequency Control*, 55 (12), 2544-2551.

[28] Man Bok Hong, Yung-Ho Jo. (2012). Design and evaluation of 2-DOF compliant forceps with force-sensing capability for minimally invasive robot surgery. *IEEE Transactions on Robotics,* 28 (4), 932-941.

[29] Dong, W., Sun, L., Du, Z. (2008). Stiffness research on a high-precision, large-workspace parallel mechanism with compliant joints. *Precision Engineering,* 32 (3), 222-231.

[30] Paros, J.M., Weisbord, L. (1965). How to design flexure hinges. *Machine Design*, 37, 151-156.

[31] Smith, S. (2000). *Flexures: Elements of Elastic Mechanisms*. New York: Gordon and Breach Science Publishers.

[32] Boyes, W. (2009). *Instrumentation Reference Book*, 3rd Edition. Burlington, MA: Elsevier.

[33] Sameer A. Joshi. (2002). *A comparative study of two classes of 3-DOF parallel manipulators*. Ph.D. dissertation, Department of Mechanical Engineering, University of Maryland, College Park, MD.

[34] Ouyang, P.R. (2005). *Hybrid intelligent machine systems: Design, modeling and control*. Ph.D. dissertation, University of Saskatchewan, Canada.

[35] Liang, Q., Zhang, D., Song, Q., Ge, Y. (2010). Micromanipulator with integrated force sensor based on compliant parallel mechanism. In *Robotics and Biomimetics (ROBIO 2010)*, 14-18 December 2010. IEEE, 709-714.

[36] Puangmali, P. et al. (2012). Miniature 3-axis distal force sensor for minimally invasive surgical palpation. *IEEE/ASME Transactions on Mechatronics*, 17 (4), 646-656.

[37] Bicchi, A. (1992). A criterion for optimal design of multi-axis force sensors. *Robotics and Autonomous Systems*, 10 (4), 269-286.

Received January 14, 2013.
Accepted October 17, 2013.